

# Critical Role of Functional Groups Containing N, S, and O on Graphene Surface for Stable and Fast Charging Li-S Batteries

Jinhua Sun, Jang-Yeon Hwang,\* Piotr Jankowski, Linhong Xiao, Jaime S. Sanchez, Zhenyuan Xia, Suyeong Lee, Alexandr V. Talyzin, Aleksandar Matic, Vincenzo Palermo,\* Yang-Kook Sun,\* and Marco Agostini\*

Lithium-sulfur (Li-S) batteries are considered one of the most promising energy storage technologies, possibly replacing the state-of-the-art lithium-ion (Li-ion) batteries owing to their high energy density, low cost, and eco-compatibility. However, the migration of high-order lithium polysulfides (LiPs) to the lithium surface and the sluggish electrochemical kinetics pose challenges to their commercialization. The interactions between the cathode and LiPs can be enhanced by the doping of the carbon host with heteroatoms, however with relatively low doping content (<10%) in the bulk of the carbon, which can hardly interact with LiPs at the host surface. In this study, the grafting of versatile functional groups with designable properties (e.g., catalytic effects) directly on the surface of the carbon host is proposed to enhance interactions with LiPs. As model systems, benzene groups containing N/O and S/O atoms are vertically grafted and uniformly distributed on the surface of expanded reduced graphene oxide, fostering a stable interface between the cathode and LiPs. The combination of experiments and density functional theory calculations demonstrate improvements in chemical interactions between graphene and LiPs, with an enhancement in the electrochemical kinetics, power, and energy densities.

## 1. Introduction


New electrochemical energy storage systems are urgently needed to meet the ever-growing needs of the portable electronics market. Among emerging energy storage technologies, lithium-sulfur (Li-S) batteries are considered the best candidate to replace commercial lithium-ion (Li-ion) batteries (LiBs). Despite its higher theoretical energy density (2600 Wh kg<sup>-1</sup>), abundance, low cost, and non-toxicity,<sup>[1,2]</sup> practical applications of sulfur have been restricted by concerns related to the lithium/sulfur reaction.<sup>[3,4]</sup> Sulfur and its end-discharge products, that is, Li<sub>2</sub>S<sub>2</sub>/Li<sub>2</sub>S, are intrinsic insulators and poorly soluble in the battery electrolyte.<sup>[5]</sup> By contrast, the intermediate discharge products such as Li-polysulfides (LiPs) are soluble in the electrolyte, enabling more efficient use of

Dr. J. Sun, Dr. J. S. Sanchez, Dr. Z. Xia, Prof. V. Palermo  
Department of Industrial and Materials Science  
Chalmers University of Technology  
Göteborg 41296, Sweden  
E-mail: palermo@chalmers.se

Dr. J.-Y. Hwang, S. Lee  
Department of Materials Science and Engineering  
Chonnam National University  
77 Yongbong-ro, Buk-gu, Gwangju 61186, South Korea  
E-mail: hjy@jnu.ac.kr

Dr. P. Jankowski  
Faculty of Chemistry  
Warsaw University of Technology  
Warsaw 00-664, Poland

Dr. P. Jankowski  
Department of Energy Conversion and Storage  
Technical University of Denmark  
Kgs. Lyngby 2800, Denmark

 The ORCID identification number(s) for the author(s) of this article can be found under <https://doi.org/10.1002/smll.202007242>.

© 2021 The Authors. Small published by Wiley-VCH GmbH. This is an open access article under the terms of the Creative Commons Attribution License, which permits use, distribution and reproduction in any medium, provided the original work is properly cited.

Dr. L. Xiao  
Department of Chemistry  
Umeå University  
Umeå 90187, Sweden

Dr. Z. Xia, Prof. V. Palermo  
Institute of Organic Synthesis and Photoreactivity (ISOF)  
CNR  
via Gobetti 101, Bologna 40129, Italy

Prof. A. V. Talyzin  
Department of Physics  
Umeå University  
Umeå 90187, Sweden

Prof. A. Matic, Dr. M. Agostini  
Department of Physics  
Chalmers University of Technology  
Göteborg 41296, Sweden  
E-mail: agostini@chalmers.se

Prof. Y.-K. Sun  
Department of Energy Engineering  
Hanyang University  
Seoul 04763, South Korea  
E-mail: yksun@hanyang.ac.kr

DOI: 10.1002/smll.202007242

the active material, but with possible migration to the surface of the Li anode and partially back to the cathode. This is called the “shuttle effect,” which causes the loss of active material and subsequent reduction of battery cycle life.<sup>[6,7]</sup>

In the last decades, many studies have attempted to integrate sulfur into carbon-based nanostructures to address the problems of low electronic conductivity and shuttle effect.<sup>[8–12]</sup> The specific capacity of Li-S was increased in the first few cycles because of the improved conductivity obtained by integrating sulfur into the carbon nanostructure. However, the nonpolar surface of carbons was not successful in retaining the dissolution of polar LiPs upon long cycling time.<sup>[7]</sup> Although S<sub>8</sub> is nonpolar and can be adsorbed relatively well by carbon materials, Li<sub>2</sub>S and LiPs are polar and adsorb poorly in hydrophobic hosts.<sup>[13]</sup> Furthermore, the inner confinement of sulfur in the carbon matrix limited the diffusion of Li<sup>+</sup> to a small portion of active material.<sup>[14]</sup>

Free-standing porous carbon hosts have been proposed to exploit a larger portion of the active material at the sulfur cathode, increase the conductivity of the sulfur cathode, and avoid the use of non-conductive binders (e.g., polyvinylidene fluoride (PVDF)), which modifies the porous structure of carbon, which is essential for enduring volume changes (≈80%) upon cycling.<sup>[15–17]</sup> The hydrophobic surface of carbon should be modified to improve its interaction with soluble LiPs. Metals or metal oxides are polar groups that can have a strong chemical interaction with LiPs.<sup>[18,19]</sup> Although introducing polar particles in the sulfur host can improve the cycling stability, that increases the weight of the sulfur host and furthermore, a large part of these particles are embedded in the bulk and there is no guarantee of their presence on the carbon surface; thus, the interactions with LiPs are limited.<sup>[13]</sup>

An alternative approach was proposed by introducing amphiphilic polymers (e.g., polyvinylpyrrolidone (PVP)) on the surface of carbon materials.<sup>[20]</sup> The strong binding energy (BE) between LiPs and N-methyl-2-pyrrolidone provides carbon/PVP composites with good capacity retention (80% after 300 cycles). Besides the epoxy group at the side chain of PVP, the carbon backbone and pyrrole ring have a minor contribution to restraining the dissolution of LiPs. As they are not active materials, their presence in the electrode decreases the practical energy density of the final Li-S cell.

Direct grafting of small and polar functional groups on the surface of the host would be more favorable for building the Li-S cell at the practical energy density level. This method permits the diversification of the organic functionalities attached with no large modification of the host conductivity, structure, and porosity.<sup>[20,21]</sup> In the next step, the size of the functional groups can be reduced and simplified to a single atom similar to doping of carbon materials. Previous studies showed the benefits of heteroatom doping on carbon, in particular using N atom, leading to strong interactions with LiPs.<sup>[14]</sup> Nevertheless, there are only a limited number of elements (e.g., N, S, and O) that can be included as dopants into carbon materials, and it is still a challenge to reach a high doping content (typically doping is <10%), which guarantees the presence of the dopant on the carbon surface.<sup>[22–25]</sup> By taking advantage of the tunable chemistry and variety of potential functional groups, we can instead tune the surface properties of carbon materials by covalently grafting the most suitable one to their surface. Thus, understanding the interactions of LiPs with a specific functional

group at the molecular level is important for selecting suitable molecules that can improve both the energy density and cycling stability of Li-S batteries.

In this study, the performance of Li-S batteries was enhanced by directly functionalizing the surface of the graphene-based substrate with versatile molecules. A benzene ring with variable functional groups was covalently grafted on the surface of expanded reduced graphene oxide (eRGO) using diazonium chemistry. Nitrobenzene and benzene sulfonate were selected as model molecules to understand their interaction with LiPs by combining electrochemical tests and density functional theory (DFT) calculations at the molecular level. The results demonstrate how the presence of vertical nitro- or sulfonate benzene molecules (≈1 nm high) on the surface of graphene facilitates the binding with LiPs and thus stabilizes the performance of Li-S cells reaching practical energy and power densities.

## 2. Results and Discussion

### 2.1. Modification of Surface Properties of Expanded Reduced Graphene Oxide Host

Graphene is a highly conductive nanomaterial, which has been extensively reported as a conductive additive and support for the preparation of electronic compounds.<sup>[26]</sup> In this study, eRGO was used as a conductive substrate to investigate the role of specific functional groups in the electrochemical performance of Li-S batteries. The nitrobenzene and benzene sulfonate were grafted on the eRGO surface by diazonium chemistry. We used 4-nitrobenzene diazonium tetrafluoroborate and 4-sulfonic acid phenyl diazonium tetrafluoroborate to obtain nitrobenzene functionalized eRGO (NG) and benzene sulfonate functionalized eRGO (SG), respectively (**Figure 1a**). The porous structure of eRGO with the 3D network was preserved after functionalization (Figure S1, Supporting Information). Among potential functionalities, we investigated the effect of the nitro group and sulfonate group on the performance of Li-S cells because 1) nitrogen doping has been demonstrated to effectively enhance the interactions between carbon and sulfur upon battery cycling; and 2) sulfonate group has an affinity for LiPs species formed during the electrochemical process. Further details related to the grafting and synthesis procedure are presented in the experimental section.

To confirm the success of the covalent functionalization of graphene, surface chemical compositions of synthesized NG and SG together with the precursor eRGO were characterized by X-ray photoelectron spectroscopy (XPS) (Figure 1b). No traces of N 1s were observed in the eRGO sample, while two peaks at 406 and 400.5 eV appeared in NG (middle graph of Figure 1b). The main N 1s peak at 406 eV was assigned to nitro groups. Previous work reported that nitro groups can be converted into amino groups by X-ray irradiation during XPS measurements. Therefore, an N 1s associated with the amino groups was also present in the NG sample besides the -NO<sub>2</sub> group.<sup>[27]</sup> The atomic content of N derived from the XPS analysis of the NG sample was 5.5%, indicating a high density of nitrobenzene functional groups on the surface of eRGO (1 nitrobenzene group per 7 C atoms of eRGO). A slight self-polymerization of nitrobenzene diazonium salt might happen during the synthesis, due to the

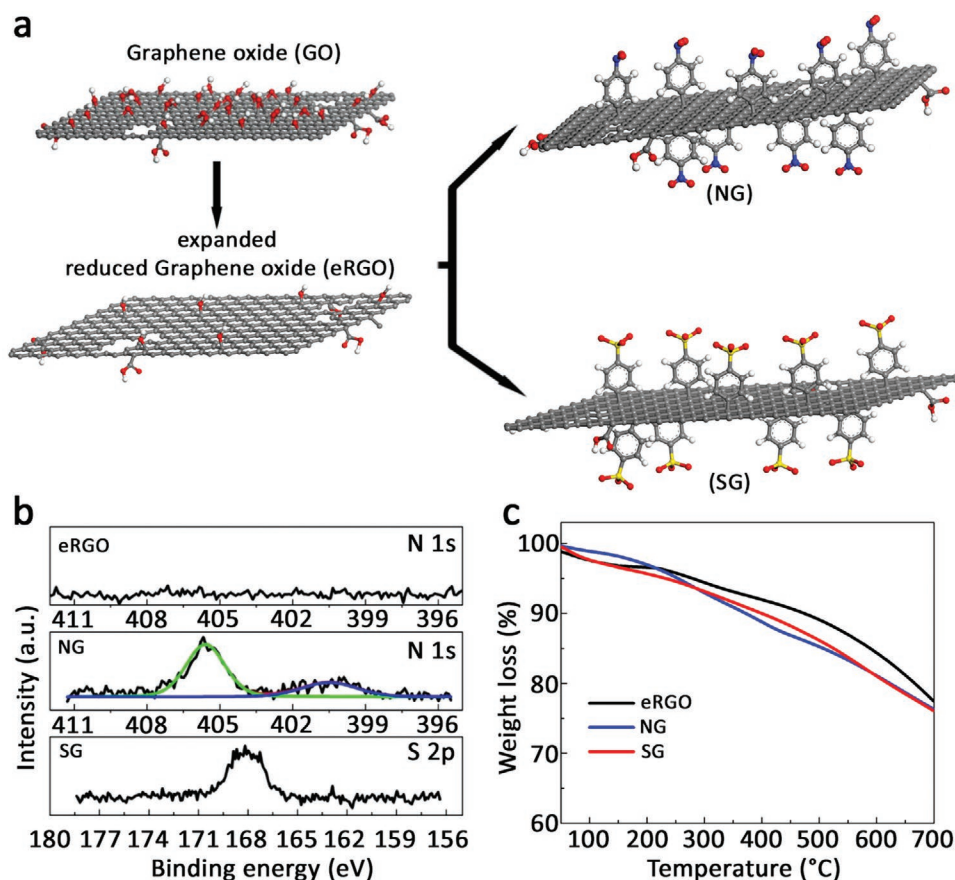


**Figure 1.** Symmetric functionalization of eRGO substrate. a) Schematic synthesis of NG and SG by diazonium chemistry. b) XPS-spectra at N 1s core level of eRGO (up) and NG (middle) samples; S 2p core-level XPS spectrum of SG (bottom). c) TGA analysis for eRGO, NG, and SG samples, under Ar.

high reactivity of aryl radicals generated from the diazonium salt.<sup>[28]</sup> The XPS analysis at the S 2p core level for the SG sample also showed the presence of an intense peak at 168 eV (bottom of Figure 1b) (4.6% in atomic content), demonstrating the covalent grafting of sulfonate benzene group on the pristine sample (1 benzene sulfonate group per 9C atoms of eRGO).<sup>[29]</sup>

The loading of nitrobenzene and benzene sulfonic acid functional groups on NG and SG was calculated using thermogravimetric analysis (TGA) (Figure 1c). No obvious weight loss was observed at 150–300 °C for NG, SG, and eRGO. This is a typical temperature range where graphene oxide (GO) loses oxygen-containing functional groups. The lack of any peak in TGA indicates that eRGO had lower defectivity of GO.<sup>[30]</sup>

Functionalized NG and SG samples showed a larger weight loss ( $\approx 10\%$ ) than eRGO during TGA between 350 and 600 °C due to the decomposition of nitrobenzene and benzene sulfonic acid functional groups from NG and SG, respectively. A similar functionalization degree obtained with both molecules indicates that the nitro or sulfonate group has a minor effect on the grafting process, which is instead governed by the diazonium tetrafluoroborate moiety present in both molecules. Weight loss in all three samples above 600 °C was caused by the gradual decomposition of the eRGO defective graphene structure. The uniform distribution of both nitrobenzene and benzene sulfonate functional groups on

the surface of graphene was also confirmed by energy dispersive spectroscopy (EDS) mapping (Figures S2–S4, Supporting Information).

The surface area and porous structure are important factors that can affect not only the sulfur loading, but also the final energy density; thus, we investigated whether grafting of both nitrobenzene and benzene sulfonate groups on the eRGO substrate would affect the surface area and porosity of the substrate.<sup>[31]</sup> We characterized eRGO, NG, and SG using Brunauer–Emmett–Teller (BET) analysis (Figure S5, Supporting Information), which yielded specific surface areas of 430, 170, and 180  $\text{m}^2 \text{g}^{-1}$ , respectively. The smaller surface area was attributed to the presence of functional groups and to the collapse of macropores during solution processing. A large surface area can be beneficial in Li-S cells to increase the interaction of the electrolyte with active materials, while a small surface area enables reduction of the volume of the electrolyte required for wetting the electrode with benefit for the galvanostatic cycling performance of Li-S cells at a practical level.

## 2.2. Li/S Cells: Cycling and Rate Performance

Our approach aims in designing sulfur electrodes at a practical level. Thus, instead of infiltrating elemental sulfur ( $\text{S}_8$ ) which is

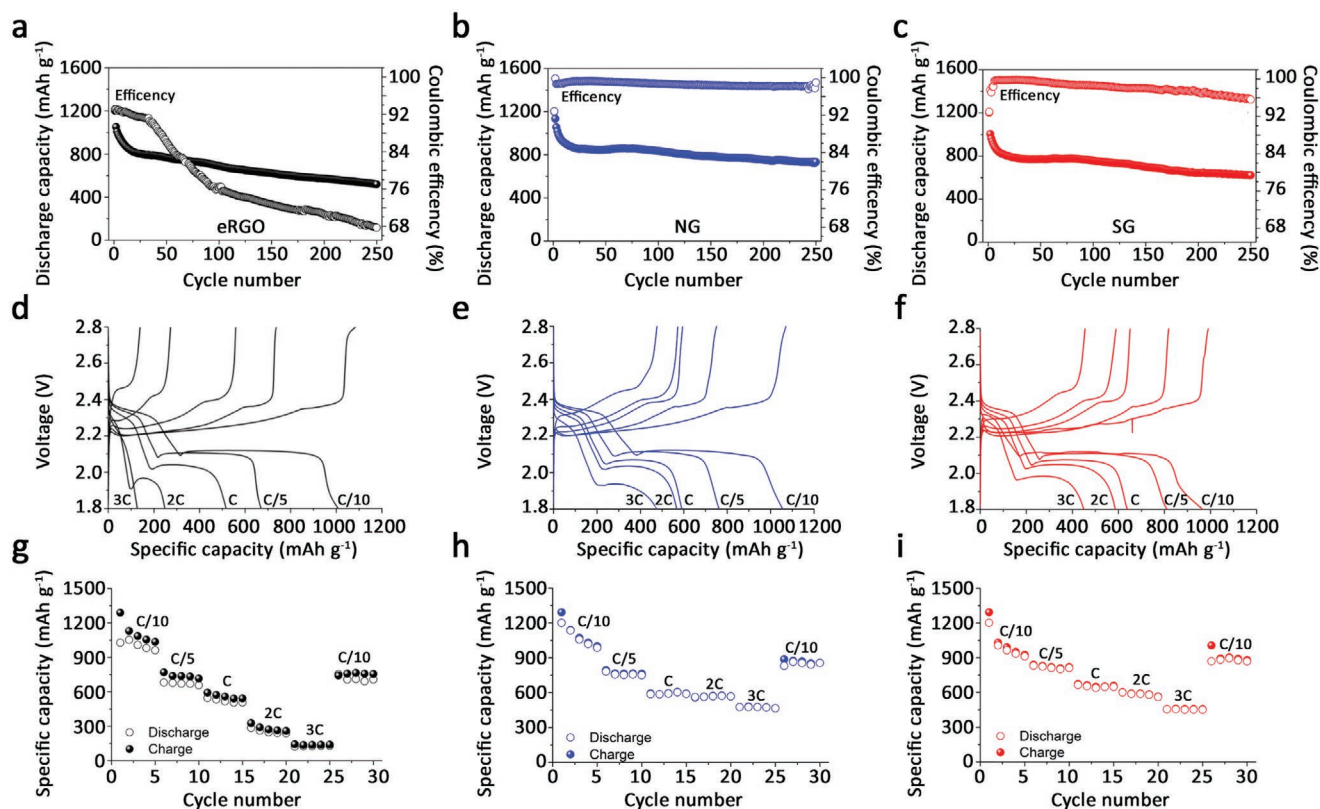


**Figure 2.** Galvanostatic cycling performance of Li/S cells made by eRGO, NG, and SG. Discharged specific capacity upon prolonged cycling number and related Coulombic efficiency at C/10 current density, for Li/S cells using a) eRGO, b) NG, and c) SG hosts. Voltage profiles at different current densities for the d) eRGO, e) NG, and f) SG Li/S cells (see in the inset the graph for values). Corresponding rate capability response for the g) eRGO, h) NG, and i) SG Li/S cells. Voltage limits: 1.8–2.8 V; (1C = 1675 mA g<sup>-1</sup>).

complicated and require the use of thermal treatment, we infiltrated a fixed amount of Li<sub>2</sub>S<sub>n</sub> polysulfides in the eRGO, NG, and SG samples by simple solvent casting technique, to achieve a high sulfur loading (i.e., 4.5 mg cm<sup>-2</sup>) in the cathode and low sulfur to electrolyte (S/E) ratio (i.e., 1:5) in the Li-S cell. We then performed galvanostatic tests of Li-S cells at the C/10 current rate (Figure 2). During the first cycle when the Li-S cells were assembled by using eRGO, we discharged/charged NG and SG at a relatively low current, that is, C/20, to convert Li<sub>2</sub>S<sub>n</sub> into Li<sub>2</sub>S and further facilitate the recovery back to S<sub>8</sub> during charging. At the first cycle, the Li/S cell built with pristine eRGO showed a Coulombic efficiency of 86% while the cells made by NG and SG revealed higher Coulombic efficiencies of 92 and 93%, respectively (Figure S6, Supporting Information). This difference was due to the larger conversion of Li<sub>2</sub>S<sub>n</sub> present in the functionalized eRGO into Li<sub>2</sub>S.

All Li-S cells were then cycled at the C/10 current rate. The one using eRGO as the sulfur host delivered an initial specific capacity of ≈900 mAh g<sup>-1</sup>, which decreased to lower values upon cycling, reaching 450 mAh g<sup>-1</sup> at cycle 250 (Figure 2a). The cell-based on the NG host delivered a higher initial specific capacity of 1200 mAh g<sup>-1</sup> decreasing to ≈750 mAh g<sup>-1</sup> at cycle 250 (Figure 2b). The Li/S cell using the SG electrode exhibited stability similar to that using NG but with a slightly different behavior during the first few cycles where the capacity quickly dropped and stabilized to values ranging between 800

and 700 mAh g<sup>-1</sup> from cycle 100 to 250 (Figure 2c). It has to be highlighted that no one of the reported Li/S cells could reach a delivered capacity as close as to the theoretical value of Li/S, that is, 1675 mAh g<sup>-1</sup>. That is mostly related to the fact that the Li/S cells are built using low sulfur to electrolyte ratio (1:5), which causes lower amount of active material reacting with Li, with consequent value of delivered specific capacity lower than the theoretical.<sup>[15,17,32]</sup>

The effect of NG and SG groups was even more apparent when rate capability tests were used. We started from a current density of C/10 and subsequently increased the rate in four steps up to 3C. The capacity of the Li/S cell using the eRGO electrode decayed quickly especially at high current rates, reaching ≈150 mAh g<sup>-1</sup> at 3C (Figure 2d,g). The voltage/capacity profile (Figure 2d) shows a large increase in voltage polarization.

A final test at the C/10 rate showed a capacity of 750 mAh g<sup>-1</sup>, less than 70% of the initial one, indicating irreversible damage to the device. In contrast, the two Li-S cells using the functionalized graphene showed capacity values in the range of battery applications at high C rates. Indeed, the NG and SG electrodes delivered a capacity of 500–450 mAh g<sup>-1</sup> even at 3C, (Figure 2e,f).

Note that the charging time at 3C is 20 min, which is important for the application in the automotive industry. Moreover, when the current density was switched back to the initial value of C/10, both electrodes recovered almost 95% of the capacity delivered at cycle 5, further demonstrating high cycling stability

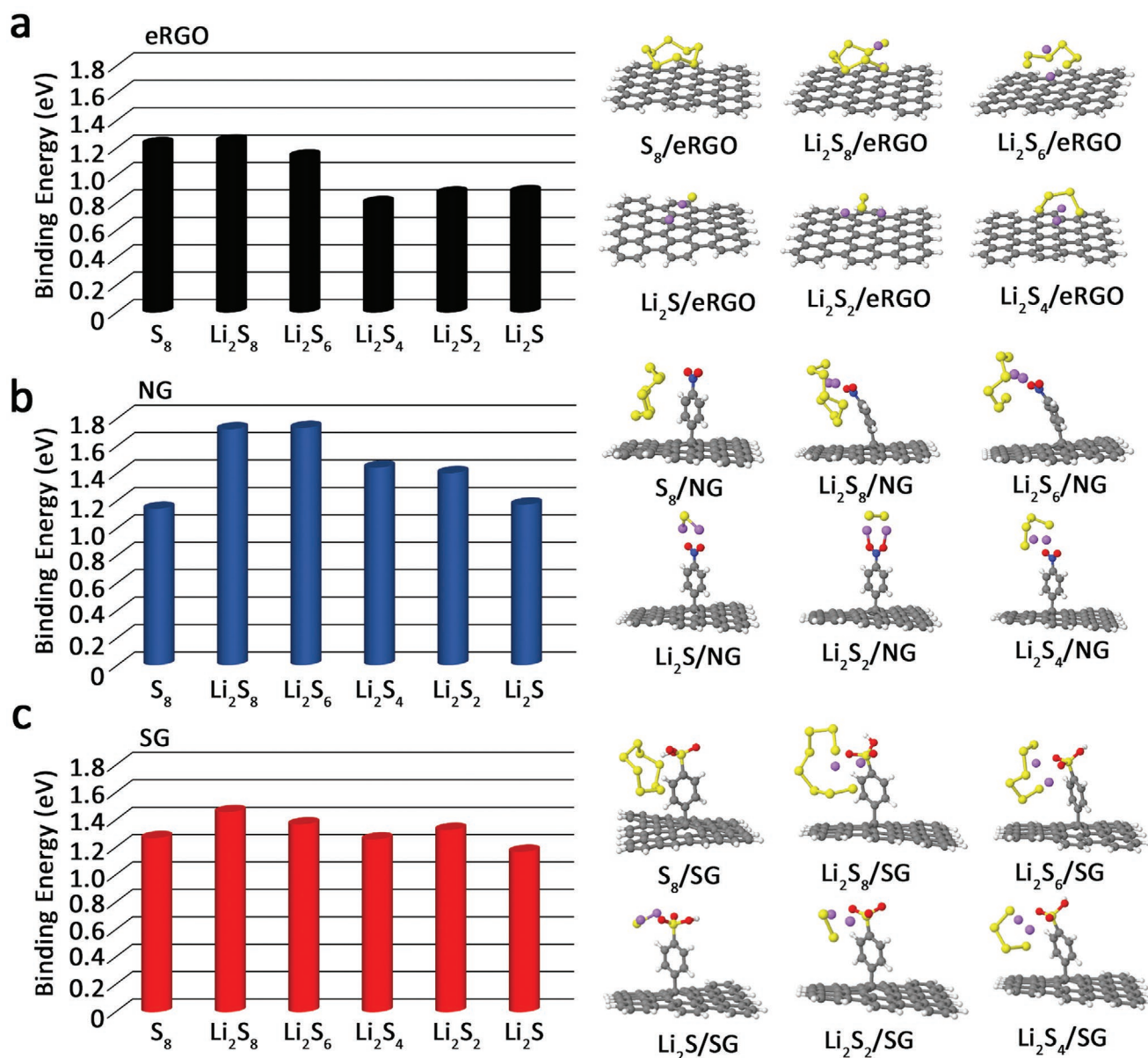


**Figure 3.** BEs and structures motif. Strength of interactions between different LiPs species and a) eRGO, b) NG, and c) SG substrate, and corresponding optimized structures.

at high C rates (Figure 2h,i). The improved performance of NG and SG as compared to eRGO was attributed to the presence of nitro and sulfonate functional groups on the surface of graphene, fostering stronger interaction with LiPs and faster Li diffusion to the electrode, improving the utilization of the active material at higher C rates, even for prolonged cycles at 2C, see Figure S7, Supporting Information.

### 2.3. Binding Interactions Between Functionalized Graphene and Li-Polysulfides Polar Species

The experiments showed that the presence of N- and S-based functional groups improved the stability and cyclability of the

material, which could be attributed to the strong polar–polar interaction between LiPs and vertical nitrobenzene and benzene sulfonate functional groups.<sup>[33]</sup> To confirm this assumption and explain the differences observed in the experiments, the interactions of sulfur and LiPs with eRGO, NG, and SG hosts were evaluated via DFT calculations. The unmodified carbon surface was modeled with a  $C_{54}H_{20}$  system consisting of 18 aromatic rings. The details of the bonding motifs, methods, and models are presented in the experimental section. We studied the BEs of eRGO, NG, and SG with LiPs with different Li:S ratios. The different chemical species present in the device during charging/discharging, from  $S_8$  to different  $Li_2S_n$  with  $1 \leq n \leq 8$  were investigated systematically (Figure 3). DFT calculations demonstrated that the NG and SG groups are

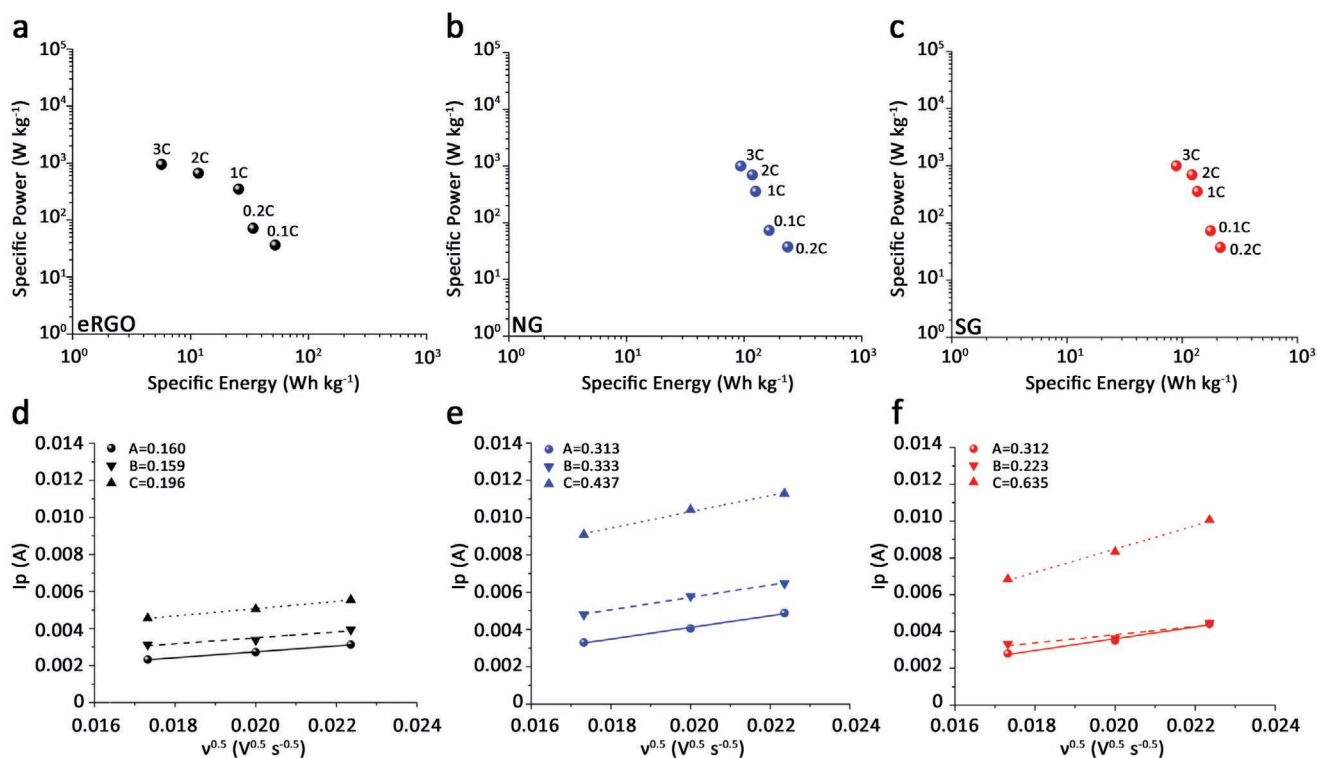


**Figure 4.** Specific energy and power densities: Ragone plots. Specific power versus specific energy calculated at different current rates (0.1, 0.2, 1, 2, and 3C) for Li/S cells using a) eRGO, b) NG, and c) SG carbon hosts. The calculation considered the total Li/S cells weight, that is, cathode, aluminum support, separator, electrolyte, and lithium weights. Linear fitting of the  $I_p$  versus scan rate for determining the  $\text{Li}^+$  diffusion coefficient for d) eRGO, e) NG, and f) SG.

oriented vertically on the graphene surface and can interact with polysulfides.

Although the eRGO substrate is expected to have the highest BE with  $\text{S}_8$  because both eRGO and  $\text{S}_8$  are nonpolar species, eRGO and SG showed comparable binding with  $\text{S}_8$  (1.23 and 1.27 eV, respectively), while BE of  $\text{S}_8$  with NG was slightly lower (1.14 eV) (Figure 3). DFT showed that this is related to the weak interaction between sulfur and OH groups, which results in lower energy achieved for the NG system.<sup>[34]</sup>

The BE of interaction of  $\text{Li}_2\text{S}_8$  with NG (= 1.72 eV) and SG (= 1.46 eV) were significantly larger than the BE with eRGO substrate (= 1.25 eV), (Figure 3a–c). The difference was more striking for interaction with  $\text{Li}_2\text{S}_n$  having higher Li content ( $n = 6, 4, 2$ , and 1) and thus higher polarity. Indeed, eRGO showed weaker interactions with polar  $\text{Li}_2\text{S}_n$  species (40–50% lower BEs weaker than  $\text{Li}_2\text{S}_8$ ) (Figure 3a). Instead, NG and SG highlighted stronger interactions, suggesting that the functional groups may improve the stability of such species on the substrate surface. The added functional groups actively participate in the immobilization of  $\text{Li}_2\text{S}_n$  species with the coordination of lithium cation by strongly electronegative atom(s); main interactions were with two oxygen atoms from the  $\text{SO}_3$  group in the SG sample, and with the nitrogen atom of  $\text{NO}_2$  in the NG sample, respectively. Therefore, a larger fraction of sulfur can be electrochemically active during the redox reaction, avoiding undesired LiPs “shuttling” to the anode surface, which agrees with the better response to the galvanostatic cycling shown in Figure 2. The  $\text{Li}_2\text{S}_n$  adsorption of

the carbon materials has been also tested visually by soaking 1 g of eRGO, NG, and SG in 10 mL of 1M  $\text{Li}_2\text{S}_8$  dimethoxyethane (DME) solution, Figure S8, Supporting Information. The Figure highlights how the NG and SG carbons are able to fully adsorb the polysulfide contained in the solution, while the bottle containing the eRGO still evidences the presence of polysulfide species in the solution. The binding of polysulfides to functionalized eRGO was further analyzed using the Fukui functions, (Figure S9, Supporting Information). The Figure highlights interactions of  $\text{Li}_2\text{S}_x$  polysulfide mostly with functional groups (i.e.,  $-\text{NO}_2$  and  $\text{SO}_3$ ), rather than graphene layer, in the case of the functionalized carbons. Increases in electron density at Li-bonding oxygen atoms is observed, together with the decrease of electron density at the aromatic ring, indicating a shift of electron density within the functional group attached to the carbon.

#### 2.4. Specific Energy and Power Densities at Practical Level

Figure 4 shows the specific energy and power density delivered at different current rates. Differently from previous studies, we calculated all the values considering the total weight of the built Li-S cells produced, including electrodes, electrolytes, separators, and current collectors.<sup>[35]</sup> Energy density and power density are often calculated by considering only part of the cell components, which generates higher apparent density. We think that it is more appropriate to use the total weight of the

device based on Table S1, Supporting Information. Figure 4a shows the Ragone plots of the eRGO electrode; specific power and energy densities of eRGO are worse than those of commercial Li-ion systems both at lower and higher current rates.<sup>[36]</sup> By contrast, Li-S cells made by NG and SG carbon hosts show a Ragone plot with enhanced specific power and energy densities (Figure 4b,c). The performance of both cells is comparable to that of Li-metal cells at low C rates<sup>[37]</sup> and better than that of Li-metal cells at high C rates.<sup>[38]</sup>

To understand whether this improvement was caused by an improvement of reaction kinetics, we carried out cyclic voltammetry (CV) tests at different scan rates (Figure S10, Supporting Information). The current values for different redox peaks (A, B, and C in CV tests) were plotted as a function of the square root of the scan rate (Figure 4d–f). Then, a linear fitting was applied and the Randles–Sevcik equation was used to calculate the  $\text{Li}^+$  diffusion coefficient ( $D_{\text{Li}^+}$ ) at different stages of discharge/charge.<sup>[39]</sup> According to the Randles–Sevcik equation, the  $D_{\text{Li}^+}$  values at the cathodic (A and B) and anodic (C) peaks of the Li-S cell using the pristine eRGO electrode were of the order of  $10^{-9} \text{ cm}^2 \text{ s}^{-1}$ . When employing the NG and SG electrodes, the calculated  $D_{\text{Li}^+}$  values increased by one order of magnitude relative to pristine eRGO (Table S2, Supporting Information), showing sharper redox peaks and narrower peak separation (Figure S10, Supporting Information). This indicates that the better battery performance observed in NG and SG (as compared to eRGO) can be attributed to improved redox kinetics and higher  $\text{Li}^+$  diffusion coefficient.

### 2.5. Electrochemical Mechanism of LiPs on Functionalized Graphene Host

To gain more insight into electrochemical stability, XPS was employed to understand the evolution of different chemical species on the graphene surface. **Figure 5a** shows the voltage profile during the first discharge cycle, with red, and black dots marking the beginning and end of the cycle, respectively, indicating the state where the XPS analysis was performed for all samples.

In the S2p spectrum, the eRGO electrode showed two main peaks at 159.9 and 162.2 eV, corresponding to the long-, medium-, and short-chain polysulfide species deposited on its surface at the pristine state (Figure 5b left). Similar peaks appeared in the NG electrode (Figure 5c left), while SG showed additional peaks at 159.5 eV owing to the formation of additional  $\text{Li}_2\text{S}_n$  species and a peak at 163.2 eV related to the presence of thiosulfate groups on the graphene surface.<sup>[40]</sup>

Thus,  $\text{Li}_2\text{S}_n$  deposited during the synthesis phase was distributed at different chain lengths as a result of a disproportionation reaction that occurred during the formation of  $\text{Li}_2\text{S}_8$  in the DME solvent. After the Li-S cell was fully discharged, the pristine eRGO electrode revealed a shift of both aforementioned peaks to different BEs (one peak from 159.9 to 160.1 eV, and the second from 162.2 to 161.7 eV), confirming the conversion of  $\text{Li}_2\text{S}_n$  to  $\text{Li}_2\text{S}_2$  and  $\text{Li}_2\text{S}$  (Figure 5b right). Besides this, the NG and SG samples also showed additional peak at 167.0 eV, related to the formation of  $\text{Li}_2\text{S}(\text{S})\text{O}_3$  (Figure 5c right and Figure 5d right).

The S–O bonds on the surface of both NG and SG electrodes can prevent, in part, the migration of soluble  $\text{Li}_2\text{S}_n$  to the Li-metal surface, especially during prolonged cycling, thus keeping the active material close to the cathode side.<sup>[30]</sup> The NG electrode, which has the larger formation of  $\text{Li}_2\text{S}(\text{S})\text{O}_3$ , showed better stability upon cycling (Figure 2b), while the SG electrode, with a lower concentration of  $\text{Li}_2\text{S}(\text{S})\text{O}_3$ , showed slightly worse cycling stability (Figure 2c). The pristine eRGO electrode, where the  $\text{Li}_2\text{S}(\text{S})\text{O}_3$  on the surface was not formed, was unstable, decreasing the stability upon battery cycling. The formation of S–O bonds upon discharge was further confirmed for NG and SG electrodes from the XPS at the O 1s level (Figure S11, Supporting Information), where an additional peak appeared at 527.7 eV, while the same peak was negligible in the eRGO electrode. Overall, the XPS data given are in good agreement and provide direct evidence of what is already suggested by galvanostatic, DFT, and CV results. Furthermore, the use of functionalities at the cathodic side brings to better stability of the Li anode. SEM images of the Li recovered after 250 cycles of discharge/charge at 0.1C, Figure S12, Supporting Information, clearly evidence how the surface of Li-metal is less corroded when NG and SG electrodes are employed at the cathode side, while heavy corrosion and large holes are present at the surface of the Li recovered from a Li/S cell using pristine eRGO.

## 3. Conclusions

A new pathway to improve the specific energy and power densities of Li/S cells was proposed as an alternative to doping by introducing versatile functional groups (e.g., nitrobenzene and benzene sulfonate) on the surface of highly conductive graphene-based substrates. We demonstrated that the presence of N, S, and O on the surface of an eRGO-based substrate increased the interaction between a wide range of  $\text{Li}_2\text{S}_n$  species and the surface of the electrode. The presence of nitrobenzene and benzene sulfonate functional groups suggests that 1) the increased BEs favor the interaction of sulfur, polysulfides, and sulfide species with the surface of the electrode, and 2) the faster Li diffusion on the electrode surface promotes the reaction between Li and S and brings them closer to the surface of the host, even at high current rates. These claims were confirmed by experimental observation of better cycling stability, faster charging/discharging at a current rate as high as 3C, and by higher  $\text{Li}^+$  diffusion on functionalized electrodes. By using a practical sulfur loading of  $4.5 \text{ mg cm}^{-2}$  with an electrolyte volume of only five times this weight (S/E 1:5), the Li-S cells based on NG and SG delivered capacity, energy, and power densities comparable to commercial LiBs, outperforming them at high current rates. The functionalization strategy of graphene-based sulfur host proposed in this study offers a new concept for designing practical sulfur electrodes with enhanced cycling performance.

## 4. Experimental Section

*Thermally Expanded Reduced Graphene Oxide:* Commercial GO from Graphenea was used to prepare thermally eRGO.<sup>[41]</sup> The GO powder in a glass container was heated to 320 °C for 3 min. The GO powder was expanded and exfoliated by the removal of oxygen-containing functional

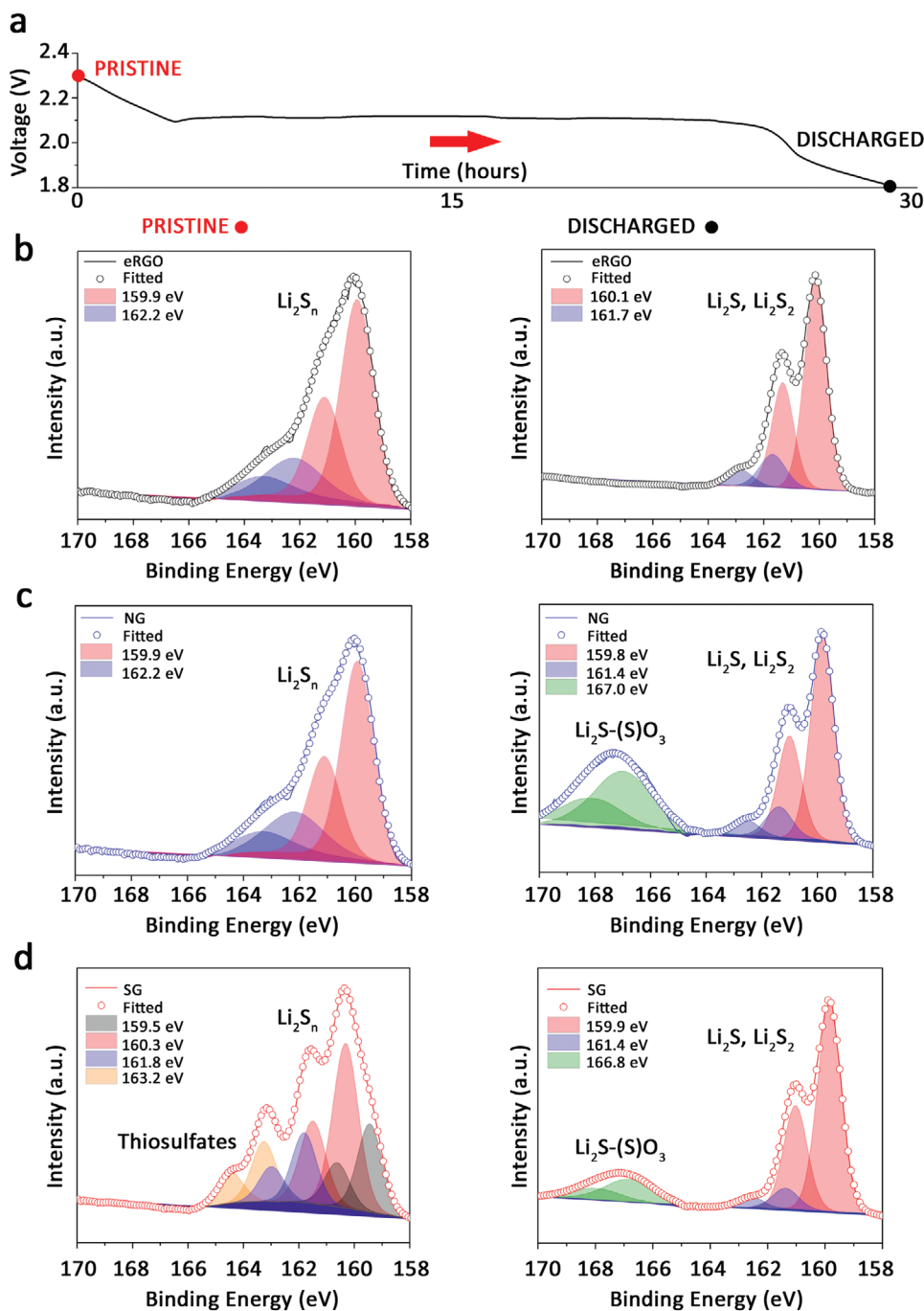


**Figure 5.** Chemical evolution of LiPs on different graphene-based hosts during battery discharge. a) Galvanostatic voltage profile measured on NG sample during the 1st discharge cycle at a current of  $C/40$  ( $IC = 1675 \text{ mA g}^{-1}$ ). XPS spectrum at the S2p core level for the b) eRGO, c) NG, and d) SG at the pristine state (red spot); after full discharge (black spot).

groups on the surface of GO. Apart from the eRGO that was synthesized in the laboratory, the commercially high surface area reduced GO, which was prepared similarly from the graphene supermarket, was also used as a starting material to synthesize NG and SG.

**Synthesis of 4-Sulfonic Acid Phenyl Diazonium Tetrafluoroborate and 4-Nitrobenzene Diazonium Tetrafluoroborate:** The two diazonium salts were synthesized according to the previously reported procedures.<sup>142</sup> First, 6 mL of tetrafluoroboric acid (48% in water) was added to 50 mL of 4-sulfanilic acid suspension (6 g); after stirring for 20 min, the mixture was cooled to 0 °C in an ice bath. Saturated sodium nitrite

(2 g) in water was then slowly added to the mixture under stirring. After 2 h reaction, the white precipitate (4-sulfonic acid phenyl diazonium tetrafluoroborate) was collected and washed with cold water. The 4-nitrobenzene diazonium tetrafluoroborate was synthesized using the same procedure, but 98% 4-nitroaniline was used as a precursor instead of 4-sulfanilic acid.

**Synthesis of NG and SG:** The as-prepared eRGO (300 mg) was first sonicated in 150 mL, 2 mg mL<sup>-1</sup> sodium dodecyl sulfate aqueous solution to allow the surfactant to penetrate the pores of eRGO. Then, 100 mg of 4-sulfonic acid phenyl diazonium tetrafluoroborate was added



stepwise to eRGO. After stirring at room temperature in the dark for 3 h, the black powder (SG) was filtrated and thoroughly washed with water and ethanol. The NG was obtained following the same procedure but by using 4-nitrobenzene diazonium tetrafluoroborate instead of 4-sulfonic acid phenyl diazonium tetrafluoroborate.<sup>[43]</sup>

**Characterization:** XPS spectra were collected using PHI VersaProbe III with a monochromatic Al K $\alpha$  source (1486.6 eV); the spot size was 100  $\mu$ m. The discharged samples were transferred directly from the glove box to the XPS chamber without exposing them to the air. The Multipak Spectrum was used for the analysis of the spectra. The BEs were calibrated using the C 1s peak at 285 eV. Surface area, pore volume, and pore size distribution were measured by nitrogen-sorption using Micromeritics TriStar 3000. Unfunctionalized sample was degassed for a minimum of 12 h at 120 °C under a N<sub>2</sub> flow. SG and NG samples were degassed for a minimum of 16 h at 120 °C under a N<sub>2</sub> flow. The surface area was calculated using the BET algorithm. Scanning electron microscopy was performed using a JEOL JSM-7800F Prime microscope equipped with EDS. TGA was performed using a Mettler Toledo TGA/DSC3+ System at a heating rate of 5 °C min<sup>-1</sup> under Ar.

**Density Functional Theory Calculations:** The pristine carbon surface was simulated using a C<sub>54</sub>H<sub>20</sub> model, consisting of 18 aromatic rings. The interactions of the resulting surfaces with different sulfur and (poly-) sulfide species (S<sub>8</sub>, Li<sub>2</sub>S, Li<sub>2</sub>S<sub>2</sub>, Li<sub>2</sub>S<sub>4</sub>, Li<sub>2</sub>S<sub>6</sub>, and Li<sub>2</sub>S<sub>8</sub>) were studied by testing at least five different starting geometries for each, prior to geometry optimization to determine the most favorable geometries. To reduce the computation time, all structures were pre-optimized using a smaller basis set (6-31G(d)) prior to the final geometry optimization using 6-311++G(d,p). The M06-2X functional, as implemented in Gaussian16 B.01, was used and shown to be appropriate for studies of graphene and carbon nanotubes.<sup>[44]</sup> The BEs were obtained by subtracting the total energy of the carbon layer-Li<sub>2</sub>S<sub>x</sub> system from the sum of the isolated carbon layer and Li<sub>2</sub>S<sub>x</sub> species optimized separately. To reduce error related to the difference in the basis set size with or without the carbon layer, the basis set superposition error correction was considered by calculating the optimized geometries of separated species in the basis set of the entire system, and the error was determined to be around 0.1 eV.

**Electrolyte and Electrodes Preparation:** The electrolyte was prepared by dissolving 0.4 mol LiNO<sub>3</sub> (Aldrich) and 1 mol of LiTFSI (Solvionic, France) in 1 L of a 1:1 volume ratio mixture of Dioxolane (DOL, Aldrich)/DME (Aldrich). Then, 1 m Li<sub>2</sub>S<sub>8</sub> solution was prepared by dissolving 2 mol of Li (Chemetall, thickness of 250  $\mu$ m) and 8 mol of sulfur (Aldrich, 99.9%) in 1 L of DME (Aldrich, 99.9%) at 80 °C. The prepared solution was stirred for about 4 h until a red-colored solution was obtained. The film electrodes were prepared on carbon-coated Al foil (Aldrich) using three powders: eRGO, NG, and SG. Seventy percent of active material (eRGO, NG, SG) was mixed with 10% PVDF (Arkema) and 20% multiwalled carbon nanotubes (MWCNTs, Aldrich) (final weight ratio of 70:10:20) and drop-casted on an Al foil (4.2 mg cm<sup>-2</sup>) using a doctor blade (film casting knife, MTI, EQ-se-KTQ-150D). The resulting 40  $\mu$ m thick films were cut into disks and dried at 80 °C under vacuum to remove the residual solvent prior to the assembly of Li-S cells. The electrode had a final weight of 6.42 mg cm<sup>-2</sup>, of which the PVDF+carbon loading was 2.22 mg cm<sup>-2</sup> (MWCNTs and corresponding carbon hosts: eRGO, NG, or SG). The 1 m Li<sub>2</sub>S<sub>8</sub> DME solution was subsequently drop-casted on the surface of the eRGO, NG, and SG electrodes at 80 °C to obtain a final Li<sub>2</sub>S<sub>8</sub> loading of 4.71 mg cm<sup>-2</sup> (sulfur = 4.47 mg cm<sup>-2</sup>). The total electrode weight was 11.15 mg cm<sup>-2</sup>.

**Electrochemical Characterizations:** The as-prepared electrodes were used in coin cell configurations together with the Celgard separator (12 mm), which was soaked with 20  $\mu$ L cm<sup>-2</sup> of electrolytes (sulfur-to-electrolyte ratio (S/E) 1:5). The cells were cycled at 1.8–2.8 V using a current density of 167 mA g<sup>-1</sup> = 0.1 C (1 C = 1675 mA g<sup>-1</sup>) for prolonged cycling tests, and 0.1, 0.5, 1, 2, and 3C for rate capability tests. All the cycling tests were performed using a Scribner 585 battery test system. CV measurements were performed using a potentiostat/galvanostat VSP (BioLogic, France) instrument in the voltage range of 1.6–2.8 V at a scan rate of 0.3, 0.4, and 0.5 mV s<sup>-1</sup>. For detecting the diffusion coefficient of

the different carbon materials, the current values at different redox peaks from CV analysis were plotted as a function of the scan rate<sup>0.5</sup>, following a linear fitting as shown in Figure 4d–f. The Li-ion diffusion coefficient was calculated using the Randles–Sevcik equation:  $I_p = 268\,600 \times e^{-1.5} \times \text{area} \times D_{\text{Li}^+} \times \text{conc.}_{\text{Li}^+} \times \text{rate}^{0.5}$ , where  $I_p$  is the current of the peak detected from CV analysis,  $e$  is the number of the electron involved in the electrochemical process, area is the cathode area,  $\text{conc.}_{\text{Li}^+}$  is the Li-ion concentration in the electrolyte, and rate is the CV scan rate.

## Supporting Information

Supporting Information is available from the Wiley Online Library or from the author.

## Acknowledgements

The research leading to these results has received funding from the European Union's Horizon 2020 research and innovation program under GrapheneCore3 881603–Graphene Flagship, FLAG-ERA project PROSPECT and MECHANICS, and from the Swedish Research Council under project Janus 2017–04456. M.A. and A.M. acknowledge support from the Chalmers Areas of Advanced Materials Science and Energy, FORMAS, and the Swedish Energy Agency. All calculations were carried out at the Wrocław Centre for Networking and Supercomputing, Grant number 346.

## Conflict of Interest

The authors declare no conflict of interest.

## Data Availability Statement

Research data are not shared.

## Keywords

electrolyte lean condition, graphene, lithium-sulfur batteries, practical energy and power density, surface functionalization

Received: November 17, 2020

Revised: January 25, 2021

Published online: March 14, 2021

- [1] A. Manthiram, Y. Fu, Y. S. Su, *Acc. Chem. Res.* **2013**, *46*, 1125.
- [2] Z. W. Seh, Y. Sun, Q. Zhang, Y. Cui, *Chem. Soc. Rev.* **2016**, *45*, 5605.
- [3] R. Kumar, J. Liu, J. Y. Hwang, Y. K. Sun, *J. Mater. Chem. A* **2018**, *6*, 11582.
- [4] Y. X. Yin, S. Xin, Y. G. Guo, L. J. Wan, *Angew. Chem., Int. Ed.* **2013**, *52*, 13186.
- [5] R. Fang, S. Zhao, Z. Sun, D. W. Wang, H. M. Cheng, F. Li, *Adv. Mater.* **2017**, *29*, 1606823.
- [6] Y. V. Mikhaylik, J. R. Akridge, *J. Electrochem. Soc.* **2004**, *151*, A1969.
- [7] V. S. Kolosnitsyn, E. V. Karaseva, *Russ. J. Electrochem.* **2008**, *44*, 506.
- [8] N. Jayaprakash, J. Shen, S. S. Moganty, A. Corona, L. A. Archer, *Angew. Chem., Int. Ed.* **2011**, *50*, 5904.
- [9] X. Ji, K. T. Lee, L. F. Nazar, *Nat. Mater.* **2009**, *8*, 500.
- [10] G. Li, J. Sun, W. Hou, S. Jiang, Y. Huang, J. Geng, *Nat. Commun.* **2016**, *7*, 10601.

- [11] S. Qi, J. Sun, J. Ma, Y. Sun, K. Goossens, H. Li, P. Jia, X. Fan, C. W. Bielawski, J. Geng, *Nanotechnology* **2019**, *30*, 024001.
- [12] J. Sun, J. Ma, J. Fan, J. Pyun, J. Geng, *APL Mater.* **2019**, *7*, 020904.
- [13] M. Agostini, A. Matic, *Small* **2020**, *16*, 1905585.
- [14] Q. Pang, X. Liang, C. Y. Kwok, L. F. Nazar, *Nat. Energy* **2016**, *1*, 16132.
- [15] J. He, G. Hartmann, M. Lee, G. S. Hwang, Y. Chen, A. Manthiram, *Energy Environ. Sci.* **2019**, *12*, 344.
- [16] L. Luo, J. Li, H. Y. Asl, A. Manthiram, *ACS Energy Lett.* **2020**, *5*, 1177.
- [17] M. Agostini, J. Hwang, H. M. Kim, P. Bruni, S. Brutti, F. Croce, A. Matic, Y.-K. Sun, *Adv. Energy Mater.* **2018**, *8*, 1801560.
- [18] X. C. Liu, S. P. Zhou, M. Liu, G. L. Xu, X. D. Zhou, L. Huang, S. G. Sun, K. Amine, F. S. Ke, *Nano Energy* **2018**, *50*, 685.
- [19] X. Tao, J. Wan, C. Liu, H. Wang, H. Yao, G. Zheng, Z. W. Seh, Q. Cai, W. Li, G. Zhou, C. Zu, Y. Cui, *Nat. Commun.* **2016**, *7*, 11203.
- [20] G. Zheng, Q. Zhang, J. J. Cha, Y. Yang, W. Li, Z. W. Seh, Y. Cui, *Nano Lett.* **2013**, *13*, 1265.
- [21] J. H. Kim, T. Kim, Y. C. Jeong, K. Lee, K. T. Park, S. J. Yang, C. R. Park, *Adv. Energy Mater.* **2015**, *5*, 1500268.
- [22] J. Song, T. Xu, M. L. Gordin, P. Zhu, D. Lv, Y. B. Jiang, Y. Chen, Y. Duan, D. Wang, *Adv. Funct. Mater.* **2014**, *24*, 1243.
- [23] J. Song, M. L. Gordin, T. Xu, S. Chen, Z. Yu, H. Sohn, J. Lu, Y. Ren, Y. Duan, D. Wang, *Angew. Chem., Int. Ed.* **2015**, *54*, 4325.
- [24] K. Park, J. H. Cho, J. H. Jang, B. C. Yu, A. T. De La Hoz, K. M. Miller, C. J. Ellison, J. B. Goodenough, *Energy Environ. Sci.* **2015**, *8*, 2389.
- [25] M. Agostini, D. H. Lim, S. Brutti, N. Lindahl, J. H. Ahn, B. Scrosati, A. Matic, *ACS Appl. Mater. Interfaces* **2018**, *10*, 34140.
- [26] F. Bonaccorso, L. Colombo, G. Yu, M. Stoller, V. Tozzini, A. C. Ferrari, R. S. Ruoff, V. Pellegrini, *Science* **2015**, *347*, 1246501.
- [27] K. Roodenko, M. Gensch, J. Rappich, K. Hinrichs, N. Esser, R. Hunger, *J. Phys. Chem. B* **2007**, *111*, 7541.
- [28] P. Huang, L. Jing, H. Zhu, X. Gao, *Acc. Chem. Res.* **2013**, *46*, 43.
- [29] S. Fleutot, H. Martinez, J. C. Dupin, I. Baraille, C. Forano, G. Renaudin, D. Gonbeau, *Solid State Sci.* **2011**, *13*, 1676.
- [30] P. Zhang, Z. Li, S. Zhang, G. Shao, *Energy Environ. Mater.* **2018**, *1*, 5.
- [31] J. Sun, F. Morales-Lara, A. Klechikov, A. V. Talyzin, I. A. Baburin, G. Seifert, F. Cardano, M. Baldrighi, M. Frascioni, S. Giordani, *Carbon* **2017**, *120*, 145.
- [32] W. Bao, L. Liu, C. Wang, S. Choi, D. Wang, G. Wang, *Adv. Energy Mater.* **2018**, *8*, 1702485.
- [33] J. Sun, A. Klechikov, C. Moise, M. Prodana, M. Enachescu, A. V. Talyzin, *Angew. Chem., Int. Ed.* **2018**, *57*, 1034.
- [34] S. J. Fretz, M. Agostini, P. Jankowski, P. Johansson, A. Matic, A. E. C. Palmqvist, *Batteries Supercaps* **2020**, *3*, 757.
- [35] B. D. McCloskey, *J. Phys. Chem. Lett.* **2015**, *6*, 4581.
- [36] R. Zhang, B. Xia, B. Li, L. Cao, Y. Lai, W. Zheng, H. Wang, W. Wang, *Energies* **2018**, *11*, 2408.
- [37] J. Y. Hwang, S. J. Park, C. S. Yoon, Y. K. Sun, *Energy Environ. Sci.* **2019**, *12*, 2174.
- [38] X. Li, J. Zheng, X. Ren, M. H. Engelhard, W. Zhao, Q. Li, J. G. Zhang, W. Xu, *Adv. Energy Mater.* **2018**, *8*, 1703022.
- [39] C. Deng, Z. Wang, S. Wang, J. Yu, D. J. Martin, A. K. Nanjundan, Y. Yamauchi, *ACS Appl. Mater. Interfaces* **2019**, *11*, 541.
- [40] D. Cai, M. Lu, L. Li, J. Cao, D. Chen, H. Tu, J. Li, W. Han, *Small* **2019**, *3*, 1902605.
- [41] A. Iakunkov, A. Klechikov, J. Sun, T. Steenhaut, S. Hermans, Y. Filinchuk, A. Talyzin, *Phys. Chem. Chem. Phys.* **2018**, *20*, 27983.
- [42] C. Saby, B. Ortiz, G. Y. Champagne, D. Bélanger, *Langmuir* **1997**, *13*, 6805.
- [43] Z. Wang, Y. Dong, H. Li, Z. Zhao, H. B. Wu, C. Hao, S. Liu, J. Qiu, X. W. D. Lou, *Nat. Commun.* **2014**, *5*, 5002.
- [44] A. Ramraj, I. H. Hillier, M. A. Vincent, N. A. Burton, *Chem. Phys. Lett.* **2010**, *484*, 295.